Analysis of high-order time-stepping schemes for nonsmooth initial conditions in financial pricing

Dawei Wang[†], Christina Christara[†∘], and Kirill Serkh[‡⋄]

December 16, 2023

Nonsmooth payoff functions are common in financial contracts and pose difficulties in obtaining high-order solutions of the contract prices. In this work, we consider convection-diffusion equations with initial conditions involving various types of nonsmoothness. We apply a fourth-order finite difference (FD) discretization on a uniform grid in space, and BDF4 time stepping initialized with two steps of an explicit third-order Runge-Kutta (RK3) method and one step of BDF3. From the Fourier analysis of the discrete system, we prove that the low-order errors generated by RK3 for nonsmooth data in the high-frequency domain get damped away by BDF steps, while low-order errors in the low-frequency domain come from the low-order initial condition discretization. To achieve globally high-order convergence, we apply fourth-order smoothing to the initial conditions, and provide explicit formulas of the discretization. By combining initial condition smoothing with the proposed time-stepping scheme, we mathematically prove and numerically verify that fourth-order convergence is obtained. Numerical examples on the model PDE and various option pricing problems are also given to demonstrate the fourth-order convergence of our method.

[†] Department of Computer Science, University of Toronto, Toronto, ON M5S 2E4

[‡] Departments of Mathematics and Computer Science, University of Toronto, Toronto, ON M5S 2E4

1 Introduction

The Black-Scholes partial differential equation (PDE) and its variants are classical models in mathematical finance. The Black-Scholes PDE

$$\frac{\partial U}{\partial t} = -\frac{\sigma^2 S^2}{2}\frac{\partial^2 U}{\partial S^2} - (r-q)S\frac{\partial U}{\partial S} + rU \tag{1}$$

solves the option price $U(t, S)$ backwards in time from a given payoff function $G(S) = U(T, S)$ at the expiry time $t = T$. This formulation assumes constant continuous dividend rate q, risk-free rate r, and volatility σ. Analytical solutions exist in this case. The payoff functions $G(S)$ in finance are often nonsmooth, such as in butterfly spread, digital call options, call/put options, and so on.

The pricing of several financial derivatives requires the solution of more complicated variants of the simple Black-Scholes equation given by (1). For such equations, there are no known analytical solutions and numerical methods are used. There is a considerable literature on the numerical methods for solving generalized Black-Scholes PDEs. However, most of the existing methods are of low order. One of the difficulties in obtaining high-order methods comes from the fact that the payoff functions in financial contracts are often nonsmooth. Such payoffs can cause a degenerated accuracy of numerical schemes as well as spurious oscillations in the approximate first and second derivatives [16, 7]. In [12], the authors investigated the convergence rate behavior of PDE methods for pricing problems with nonsmooth payoffs, and proposed various smoothing procedures (averaging the initial data, shifting the grid and a projection method) combined with a special time-stepping method suggested by Rannacher [13] to restore the expected quadratic convergence. In [12], it is shown that both the Rannacher startup procedure preceding Crank-Nicolson method, and some kind of smoothing for the initial data are necessary in order to obtain second-order convergence. In fact, with Crank-Nicolson time stepping (and the diagonal Padé schemes in general), the nonsmoothness in the initial condition causes two sources of errors: the low-order error in the high-frequency Fourier domain, and the quantization error due to the placement of the nonsmooth point on the numerical grid. The convergence behavior of Crank-Nicolson and Rannacher time-marching methods is studied in detail in [7], where the authors applied Fourier analysis to show that several implicit backward Euler steps preceding Crank-Nicolson time stepping, with suitable grid alignment of the nonsmooth point, can act as a damping device and restore the global second-order convergence. To understand the quantization error, Christara and Leung [2] analyzed the effect of the placement of the nonsmooth point relative to the grid, and of various types of smoothings of the initial conditions on the accuracy and stable second-order of convergence of the numerical methods used for solving a model convection-diffusion equation.

Higher order methods in both time and space for solving parabolic problems with nonsmooth initial data are not well investigated in the literature. Most existing studies apply grid stretching schemes combined with high-order discretization to obtain high-accuracy solutions. With either grid stretching or locally refined meshes, the grid sizes around the singularity are much smaller than on the smooth region. This provides a heuristic for improving the solution accuracy around the singularity. In [11], the authors apply a standard fourth-order FD in space with a smoothly stretched grid around the strike, and BDF4 in time. To initialize BDF4, they employ the combination of two Crank-Nicolson and one BDF3 step. With an appropriately chosen grid stretching parameter, their numerical results empirically demonstrate fourth-order

convergence in the option prices of a European vanilla call, while the convergence orders of the calculated Δ and Γ are degenerated and inconsistent. Furthermore, no theoretical guarantees of convergence and stability are provided. Indeed, the authors in [15] observe that only third-order convergence is obtained with the reference method in [11] when initializing BDF4 with two Crank-Nicolson and one BDF3 step, on a uniform space grid discretized with standard fourth-order FD, and fourth-order convergence can be restored only when initializing BDF4 with the exact solutions, which is consistent with our convergence analysis in this paper. To avoid wide stencils of standard high-order FD methods, methods that apply high-order compact (HOC) schemes, usually on uniform grids, are also commonly applied, see e.g. [15, 4, 5, 6]. In [4, 5, 6], the authors construct HOC schemes on a uniform grid to price more complicated models with stochastic volatility and jumps in multiple dimensions. To match the fourth-order accuracy in space discretization, a fourth-order smoothing operator [8] is applied to the nonsmooth payoff functions. Compared to the standard FD methods, the construction of the HOC coefficients can be restrictive and quite tedious. Moreover, these methods are typically only second-order accurate in time. To obtain highly accurate time-stepping schemes, the authors in [3] apply an exact in time exponential time integration method, combined with a high-order FD scheme on a locally refined mesh in space, though it is relatively inefficient to approximate the matrix exponential and vector product. Other lines of work based on the weighted essentially non-oscillatory (WENO) discretization schemes are also proposed to solve option pricing problems with nonsmoothness in the solutions or terminal conditions [14, 10]. These schemes are known to be of a high accuracy in smooth solution regimes, while in regions with discontinuities or large gradients, there is an automatic switch to a one-sided high-order reconstruction, which prevents the creation of spurious oscillations.

In this paper, we propose a simple to implement fourth-order method to solve parabolic PDEs with nonsmooth initial conditions. Our method applies BDF4 time stepping initialized with two steps of an explicit third-order Runge-Kutta (RK3) and one step of BDF3 schemes (we can also initialize with three steps of RK3). We prove that RK3 generates low-order errors for nonsmooth data in the high-frequency domain that can be damped away by BDF4, while low-order errors in the low-frequency domain are due to the propagation of low-order initial condition discretization. To deal with the quantization errors due to low-order, nonsmooth initial conditions, we derive explicit formulas for fourth-order smoothing of the Dirac delta, Heaviside and ramp initial conditions, from the smoothing operators suggested in [8], and use these to eliminate the low-order errors of the initial condition discretization in the Fourier domain. Given a high-order initial condition discretization, the time-stepping scheme combining RK3 in the first two time steps, BDF3 in the third time step, and BDF4 afterwards is guaranteed to be globally fourth-order in time. Our analysis can be easily generalized to even higher order time-stepping schemes in the BDF and Runge-Kutta families of methods.

This paper is organized as follows: In Section 2, we set out the model convection-diffusion equation and various nonsmooth initial conditions that our convergence analysis is based on. In Section 3, we introduce the high-order discretization schemes we use. In Section 4, we write the error of BDF4 in the Fourier domain as the sum of two terms, namely the high- and low-frequency components, and study their convergence. In Section 5, we analyze the error of RK3 in the Fourier domain, and show that it has a nonconvergent high-frequency component, which, when RK3 is followed by BDF4 (or other BDF method), is damped exponentially. In Section 6, we derive explicit expressions for the smoothed discretization of the initial conditions. In Section 7, we bring back all errors to the time domain and demonstrate fourth-order

convergence of our method. Finally, in Section 8, we present numerical experiments on both the model PDE and the European digital call, call and butterfly spread options that verify our theoretical conclusions.

2   Preliminaries

We investigate the convection-diffusion equation

$$\frac{\partial v}{\partial t} = \epsilon \frac{\partial^2 v}{\partial x^2} - a \frac{\partial v}{\partial x} \tag{2}$$

over $-\infty < x < \infty$ and $0 < t < T$, under the initial conditions

$$v(0, x) = \delta(x), \tag{3}$$

$$v(0, x) = H(x) \equiv \begin{cases} 1, & x \geq 0, \\ 0, & x < 0, \end{cases} \tag{4}$$

$$v(0, x) = \max(x, 0), \tag{5}$$

which correspond to the Dirac delta, Heaviside and ramp initial conditions, respectively. The exact solutions corresponding to the three initial conditions (3), (4) and (5) are, respectively,

$$v_\delta(t, x) \equiv \frac{1}{\sqrt{4\pi\epsilon t}} \exp\left(-\frac{(x - at)^2}{4\epsilon t}\right) = \frac{(\sqrt{2}\zeta)^{-1}}{2} \; i^{-1} \operatorname{erfc}\left(-\frac{x - at}{\sqrt{2}\zeta}\right), \tag{6}$$

$$v_H(t, x) \equiv \int_{-\infty}^{x} \frac{1}{\sqrt{4\pi\epsilon t}} \exp\left(-\frac{(y - at)^2}{4\epsilon t}\right) dy = \frac{(\sqrt{2}\zeta)^0}{2} \; i^0 \operatorname{erfc}\left(-\frac{x - at}{\sqrt{2}\zeta}\right), \tag{7}$$

$$v_C(t, x) \equiv \int_{-\infty}^{x} \int_{-\infty}^{z} \frac{1}{\sqrt{4\pi\epsilon t}} \exp\left(-\frac{(y - at)^2}{4\epsilon t}\right) dy dz = \frac{(\sqrt{2}\zeta)^1}{2} \; i^1 \operatorname{erfc}\left(-\frac{x - at}{\sqrt{2}\zeta}\right), \tag{8}$$

where $\zeta = \sqrt{2\epsilon t}$, $i^{-1} \operatorname{erfc}(x) = \frac{2}{\sqrt{\pi}} e^{-x^2}$, $i^0 \operatorname{erfc}(x) = \operatorname{erfc}(x)$, $i^1 \operatorname{erfc}(x) = \int_x^{\infty} \operatorname{erfc}(z) dz$, and $i = \sqrt{-1}$. The first and second derivatives of (6) are

$$\begin{aligned} \frac{dv_\delta}{dx} &= -\frac{x - at}{(\sqrt{2}\zeta)^3} \; i^{-1} \operatorname{erfc}\left(-\frac{x - at}{\sqrt{2}\zeta}\right), \\ \frac{d^2 v_\delta}{dx^2} &= \left(\frac{2(x - at)^2}{(\sqrt{2}\zeta)^5} - \frac{1}{(\sqrt{2}\zeta)^3}\right) \; i^{-1} \operatorname{erfc}\left(-\frac{x - at}{\sqrt{2}\zeta}\right), \end{aligned} \tag{9}$$

and the first and second derivatives of (7) and (8) are, respectively,

$$\frac{dv_H}{dx} = v_\delta, \quad \frac{d^2 v_H}{dx^2} = \frac{dv_\delta}{dx}, \tag{10}$$

$$\frac{dv_C}{dx} = v_H, \quad \frac{d^2 v_C}{dx^2} = \frac{dv_H}{dx}. \tag{11}$$

We take $\epsilon = 1$ in this paper. We are interested in approximating the solution and its derivatives to a high-order accuracy. Note that these three types of singularities form the basis of many other nonsmooth

functions. For example, the bump (a type of butterfly spread) function can be constructed from a linear combination of ramp functions, as

$$v(0, x) = \max(x - \mathcal{B}, 0) - 2 \max(x, 0) + \max(x + \mathcal{B}, 0), \tag{12}$$

where $\mathcal{B} > 0$ is a constant. A shifted version of the bump function is often seen in finance as the payoff function of a butterfly spread. The exact solution of (2) with the bump initial condition can be calculated from the same linear combination of the solutions of (2) with the corresponding ramp functions as the initial conditions.

We define the Fourier transform pair of a generic function $v(t, x)$ as

$$\hat{v}(t, \omega) \equiv \int_{-\infty}^{\infty} v(t, x) e^{-i\omega x} dx, \quad v(t, x) \equiv \frac{1}{2\pi} \int_{-\infty}^{\infty} \hat{v}(t, \omega) e^{i\omega x} d\omega.$$

The Fourier transformed model problem (2) in the frequency domain becomes $\hat{v}_t = -(\omega^2 + ia\omega)\hat{v}$, and has the exact solution

$$\hat{v}(t, \omega) = e^{-(\omega^2 + ia\omega)t} \hat{v}(0, \omega), \tag{13}$$

where $\hat{v}(0, \omega)$ is the Fourier transform of any of the initial conditions defined in (3) to (5). When it is clear from context, we drop ω in the frequency notation and simply write $\hat{v}(t)$ for convenience.

When numerically computing the solution on a grid $\{x_j\}$, for $j = \ldots, -1, 0, 1, \ldots$, the nonsmooth point does not necessarily lie exactly on a grid point. To accommodate this, we introduce a parameter $\alpha \in (0, 1]$ and denote $x_j = (j + (1 - \alpha))h$ as the grid points, where h is the uniform spatial stepsize. The nonsmooth point is fixed at $x = 0$. For general α, the delta initial condition is typically discretized as [7, 2]

$$\delta_\alpha(x_j) \equiv \begin{cases} \frac{1-\alpha}{h}, & j = -1, \\ \frac{\alpha}{h}, & j = 0, \\ 0, & \text{else}, \end{cases} \tag{14}$$

which is equivalent to second order smoothing in [8]. The discretization of (4), (5) and (12) can be simply sampled from the continuous respective function so that

$$H_\alpha(x_j) \equiv \begin{cases} 1, & j \geq 0, \\ 0, & \text{else}, \end{cases} \tag{15}$$

$$C_\alpha(x_j) \equiv \max(x_j, 0), \tag{16}$$

$$B_\alpha(x_j) \equiv \max(x_j + \mathcal{B}) - 2\max(x_j, 0) + \max(x_j - \mathcal{B}, 0). \tag{17}$$

However, it turns out that the naive discretization of initial conditions given above may lead to deterioration of the convergence rate of a high-order method, due to their low-order representation in the frequency domain. Moreover, the alignment of the nonsmooth point on the grid also plays a role in the convergence

order. In the following, we relate the discretization of the initial conditions and their convergence orders from the perspective of Fourier analysis, and propose alternative discretization schemes for the Dirac delta, Heaviside, and ramp initial conditions, in order to solve (2) with high-order methods. Since the bump function is a simple linear combination of the Heaviside functions, we mostly focus our discussion on the three basic initial conditions: the Dirac delta, Heaviside and ramp functions.

3 Discretization

Consider a discretized domain $x_0 < x_1 < \cdots < x_M$ where x_0 and x_M represent the left and right boundary respectively. Let $V_j^n \approx v(t_n, x_j)$ be the FD approximation to the true solution $V(t_n, x_j)$, where $t_n = nk$ is the n-th time step, and $k = \frac{T}{N}$ is the time step size with a total of N time steps. We drop the superscript n when time is irrelevant. On a uniform grid with stepsize h, the fourth-order FD approximation to $\frac{\partial^2 V}{\partial S^2}(t, x_j)$ is given by the operator

$$D_4^2 V_j \equiv \frac{1}{12h^2}(-V_{j-2} + 16V_{j-1} - 30V_j + 16V_{j+1} - V_{j+2}),$$

for $2 \leq j \leq M - 2$. At the boundaries, we only need to apply second-order discretization to maintain fourth-order accuracy [1],

$$D_4^2 V_1 \equiv \frac{1}{h^2}(V_0 - 2V_1 + V_2),$$

for $j = 1$, and similarly for $j = M - 1$. Note that when we need to shift the grid, the boundary stepsizes become nonuniform (not equal to h), we need to apply fourth-order discretization at the boundary too, e.g.

$$D_4^2 V_1 \equiv \frac{1}{12h^2}(10V_0 - 15V_1 - 4V_2 + 14V_3 - 6V_4 + V_5).$$

The fourth-order FD approximation to $\frac{\partial V}{\partial S}(t, x_j)$ is given by the operator

$$D_4 V_j \equiv \frac{1}{12h}(V_{j-2} - 8V_{j-1} + 8V_{j+1} - V_{j+2}),$$

for $2 \leq j \leq M - 2$, and

$$D_4 V_1 \equiv \frac{1}{h}(-V_0 + V_2).$$

for $j = 1$, and similarly for $j = M - 1$. Again, when we need to shift the grid, a fourth-order discretization is used, e.g.

$$D_4 V_1 \equiv \frac{1}{12h}(-3V_0 - 10V_1 + 18V_2 - 6V_3 + V_4).$$

For convenience of later discussion, we denote $\mathcal{D}_h$ to be $\mathcal{D}_h \equiv D_4^2 - aD_4$, so that

$$\mathcal{D}_h V_j = \frac{-V_{j-2} + 16V_{j-1} - 30V_j + 16V_{j+1} - V_{j+2}}{12h^2} - a\frac{V_{j-2} - 8V_{j-1} + 8V_{j+1} - V_{j+2}}{12h}.$$

for $2 \leq j \leq M - 2$, while slightly different relations hold for $j = 1$ and $j = M - 1$. Hence, with the space discretization of (2), we obtain an ordinary differential equation (ODE) system

$$\frac{dV_j}{dt} = \mathcal{D}_h V_j, \quad 1 \leq j \leq M - 1.$$

When using BDF4 time-stepping, with time step size k, we have, for the $(l+4)$-th time step,

$$\frac{\frac{25}{12}V_j^{(l+4)} - 4V_j^{(l+3)} + 3V_j^{(l+2)} - \frac{4}{3}V_j^{(l+1)} + \frac{1}{4}V_j^{(l)}}{k} = \mathcal{D}_h V_j^{(l+4)}, \tag{18}$$

for $2 \leq j \leq M - 2$. For later convenience, define

$$\alpha_4 = \frac{25}{12}, \ \alpha_3 = -4, \ \alpha_2 = 3, \ \alpha_1 = -\frac{4}{3}, \ \alpha_0 = \frac{1}{4}. \tag{19}$$

Hence, (18) becomes

$$\sum_{n=0}^{4} \alpha_n V_j^{(l+n)} = k\mathcal{D}_h V_j^{(l+4)}. \tag{20}$$

4 Fourier analysis of the discrete system arising from BDF4

In this section, we investigate the Fourier transform of the discretized PDE. In the following analysis, we employ the Fourier transform pair [17] to study the convergence behavior of the discretization. With the alignment $\alpha = 1$ and with $\theta \equiv \omega h$, the semi-discrete Fourier transform pair is

$$\hat{V}(\omega h) = \hat{V}(\theta) = h\sum_{j=-\infty}^{\infty} V_j e^{-i\omega x_j} = h\sum_{j=-\infty}^{\infty} V_j e^{-ij\theta}, \tag{21}$$

$$V_j = \frac{1}{2\pi}\int_{-\frac{\pi}{h}}^{\frac{\pi}{h}} \hat{V}(\omega h)e^{i\omega x_j}d\omega = \frac{1}{2\pi h}\int_{-\pi}^{\pi} \hat{V}(\theta)e^{ij\theta}d\theta, \tag{22}$$

Note that the direct application of the semi-discrete Fourier transform is only valid for the case of Dirac delta initial condition, because the summation in (21) of the semi-discrete Fourier transform of the solutions V_H and V_C corresponding to the Heaviside and the ramp initial conditions, respectively, is divergent. For

this reason, the Fourier transform pair for the Heaviside and ramp initial conditions we use here is

$$\hat{V}(\omega h) = \hat{V}(\theta) = h \sum_{j=-\infty}^{\infty} (e^{-\eta j h} V_j) e^{-i\omega x_j} = h \sum_{j=-\infty}^{\infty} (e^{-\eta j h} V_j) e^{-ij\theta},$$

$$e^{-\eta j h} V_j = \frac{1}{2\pi} \int_{-\frac{\pi}{h}}^{\frac{\pi}{h}} \hat{V}(\omega h) e^{i\omega x_j} \, d\omega = \frac{1}{2\pi h} \int_{-\pi}^{\pi} \hat{V}(\theta) e^{ij\theta} \, d\theta,$$

which requires to multiply both sides of (18) by $e^{-\eta j h}$, for $\eta > 0$, before the semi-discrete inverse Fourier transform can be applied. As a result, $\hat{V}$ is not the direct Fourier transform of the solutions in the cases of the Heaviside and the ramp initial conditions. However, for notational simplicity, we do not explicitly differentiate the two situations. Readers should understand the meaning of $\hat{V}$ from its context.

With this clarification in mind, from (20), we use (22) to get

$$\sum_{n=0}^{4} \alpha_n \hat{V}^{(l+n)}(\theta) = \mu \hat{V}^{(l+4)}(\theta), \tag{23}$$

where $\alpha_4, \alpha_3, \alpha_2, \alpha_1, \alpha_0$ are the BDF4 coefficients as defined in (19), and

$$\mu = -\frac{\bar{d}}{12} \left(2\cos(2\theta) - 32\cos\theta + 30) \right) - i\frac{ad}{12} \left(16\sin\theta - 2\sin(2\theta) \right)$$

$$= -\frac{\bar{d}}{3}(1 - \cos\theta)(7 - \cos\theta) - i\frac{ad}{3}\sin\theta(4 - \cos\theta), \tag{24}$$

where $d = \frac{k}{h}$ and $\bar{d} = \frac{k}{h^2}$. Note that a is fixed for a given problem, and $k = dh$ for some constant d. By re-arranging the terms, we can write (23) as

$$\sum_{n=0}^{4} \hat{\alpha}_n \hat{V}^{(l+n)}(\theta) = 0, \tag{25}$$

with the coefficients

$$\hat{\alpha}_4 = \frac{25}{12} + \frac{\bar{d}}{3}(1 - \cos\theta)(7 - \cos\theta) + i\frac{ad}{3}\sin\theta(4 - \cos\theta) = \alpha_4 - \mu,$$

$$\hat{\alpha}_3 = \alpha_3 = -4, \ \hat{\alpha}_2 = \alpha_2 = 3, \ \hat{\alpha}_1 = \alpha_1 = -\frac{4}{3}, \ \hat{\alpha}_0 = \alpha_0 = \frac{1}{4}. \tag{26}$$

The corresponding characteristic polynomial of the difference equation (25) is

$$\sum_{n=0}^{4} \hat{\alpha}_n \xi^n = \rho(\xi) - \mu \xi^4, \text{ where } \rho(\xi) = \sum_{n=0}^{4} \alpha_n \xi^n. \tag{27}$$

Considering the recurrence relation

$$\hat{V}^{(l+4)} = -\frac{\alpha_3 \hat{V}^{(l+3)} + \alpha_2 \hat{V}^{(l+2)} + \alpha_1 \hat{V}^{(l+1)} + \alpha_0 \hat{V}^{(l)}}{\hat{\alpha}_4}, \tag{28}$$

we find the generic expression of $\hat{V}^{(l+4)}$ given the four starting values $\hat{V}^{(l+n)}$ for $n = 0, 1, 2, 3$. To study the convergence behavior, we write the BDF4 iteration as a one-step method by

$$\bar{V}^{(l+1)} \equiv \begin{bmatrix} \hat{V}^{(l+4)} \\ \hat{V}^{(l+3)} \\ \hat{V}^{(l+2)} \\ \hat{V}^{(l+1)} \end{bmatrix} = \begin{bmatrix} -\frac{\hat{\alpha}_3}{\hat{\alpha}_4} & -\frac{\hat{\alpha}_2}{\hat{\alpha}_4} & -\frac{\hat{\alpha}_1}{\hat{\alpha}_4} & -\frac{\hat{\alpha}_0}{\hat{\alpha}_4} \\ 1 & 0 & 0 & 0 \\ 0 & 1 & 0 & 0 \\ 0 & 0 & 1 & 0 \end{bmatrix} \begin{bmatrix} \hat{V}^{(l+3)} \\ \hat{V}^{(l+2)} \\ \hat{V}^{(l+1)} \\ \hat{V}^{(l)} \end{bmatrix} \equiv R\bar{V}^{(l)}, \tag{29}$$

where $R = R(\mu)$ is a function of μ denoting the iteration matrix. The spectral radius of R indicates the convergence behavior of the iteration. Note that there is one-to-one correspondence between the roots of the characteristic polynomial $\rho(\xi) - \mu\xi^4$ and the eigenvalues of the companion matrix R.

Let $\hat{E}^{(l)} \equiv \hat{v}(t_l) - \hat{V}^{(l)}$ for $l \geq 0$, and the truncation error

$$\varepsilon^{(l)} \equiv \frac{1}{\hat{\alpha}_4} \sum_{n=0}^{4} \hat{\alpha}_n \hat{v}(t_{l+n}) \tag{30}$$

Define $\bar{E}^{(l)} \equiv [\hat{E}^{(l+3)}, \hat{E}^{(l+2)}, \hat{E}^{(l+1)}, \hat{E}^{(l)}]^T$, and $\bar{\varepsilon}^{(l)} \equiv [\varepsilon^{(l)}, 0, 0, 0]^T$. Then, we can see from the iterative scheme (29) that

$$\bar{E}^{(l+1)} = R\bar{E}^{(l)} + \bar{\varepsilon}^{(l)},$$

and therefore,

$$\bar{E}^{(l+1)} = R^{l+1}\bar{E}^{(0)} + \sum_{j=0}^{l} R^j \bar{\varepsilon}^{(l-j)},$$

given an initial approximate $\bar{V}^{(0)}$ and the corresponding $\bar{E}^{(0)}$.

Note that $\hat{V}, \hat{E}, \bar{E}, \bar{V}$ and R are (vector-)functions of ω and h. For the convenience of later discussion, for any fixed $h \in (0, 1)$, when $\omega \neq 0$, we define

$$\beta \equiv \frac{\log|\omega|}{\log(1/h)}, \tag{31}$$

so that ω and h are related by $|\omega| = h^{-\beta}$. Since $\omega \in [-\pi/h, \pi/h]$, we get that $\beta \leq 1 + \frac{\log\pi}{\log(1/h)} \equiv \beta_{\max}$. The exact solution $\hat{v}(t_N)$ at $t_N \equiv T = Nk$ is

$$\hat{v}(t_N) = e^{-(\omega^2 + ia\omega)Nk}\hat{v}(0) = e^{-(\omega^2 + ia\omega)T}\hat{v}(0).$$

For later discussion, we define $z \equiv (\omega^2 + ia\omega)k$. We see that, as $h \to 0$, we have $\hat{v}(t_N) \to e^{-\infty} = 0$ exponentially in the frequency range $|\omega| = h^{-\beta}$ with $\beta > 0$. In general, the exact solution for all t_n decays exponentially to zero when $\beta > \frac{1}{2}$. The goal is to study the stability and convergence of the BDF4 solution by investigating the behavior of $\hat{V}^{(N)}$ obtained from the recurrence relation (28). In the following discussion, we consider the frequencies $|\omega| = h^{-\beta}$ with $\beta < \frac{1}{2}$, and the frequency $\omega = 0$ as being in the

low-frequency regime, and the frequencies $|\omega| = h^{-\beta}$ with $\frac{1}{2} \le \beta \le \beta_{\max}$ as being in the high-frequency regime, as shown in Figure 1. We show later that the convergence performance of the approximate $\hat{V}^{(n)}$ behaves differently in the high and low-frequency domain.
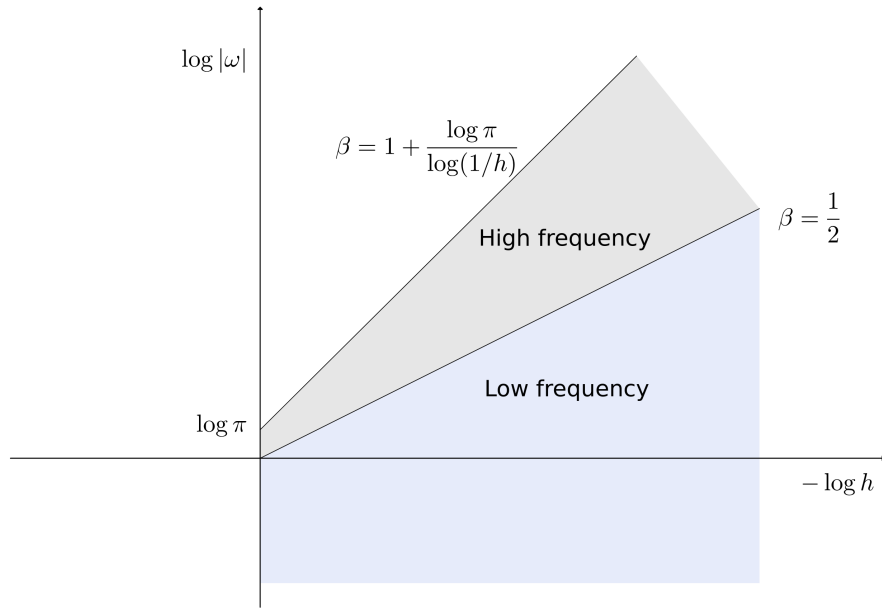

Figure 1: High- and low-frequency regions arising in BDF4. Note that $|\omega| = h^{-\beta}$.

The following lemmas are useful to prove our main theorem.

Lemma 4.1. *Let β be defined by (31), and μ be given by (24). As $h \to 0$, we have $|\mu| \to \infty$ when $\frac{1}{2} < \beta \le \beta_{\max}$; and $|\mu| \to 0$ when $\beta < \frac{1}{2}$.*

Proof. When $1 \le \beta \le \beta_{\max}$, we have $\omega h \not\to 0$ as $h \to 0$. Hence, the real part $\mathrm{Re}(\mu) = -\frac{d}{3h}(1 - \cos(\theta))(7 - \cos(\theta)) \to -\infty$, and the imaginary part $|\mathrm{Im}(\mu)| = \left| -\frac{ad}{3} \sin \theta (4 - \cos \theta) \right|$ is bounded above by a finite number. It is obvious that $|\mu| \to \infty$.

When $\beta < 1$, we have $\omega h \to 0$. In this case, $\mathrm{Im}(\mu) \to 0$. Moreover,

$$
\begin{aligned}
\lim_{h \to 0} \mathrm{Re}(\mu) &= \lim_{h \to 0} \left[-\frac{d}{3h}(1 - \cos(\theta))(7 - \cos(\theta)) \right] \\
&= -\frac{d}{3} \lim_{h \to 0} \frac{(1 - \cos h^{1-\beta})(7 - \cos h^{1-\beta})}{h} \\
&= -\frac{d}{3} \lim_{h \to 0} \frac{(1 - \beta)h^{-\beta} \sin h^{1-\beta}(8 - 2 \cos h^{1-\beta})}{1} \\
&= -2(1 - \beta)d \lim_{h \to 0} \frac{\sin h^{1-\beta}}{h^\beta} \\
&= -2(1 - \beta)d \lim_{h \to 0} h^{1-2\beta}.
\end{aligned}
$$

We see that if $\frac{1}{2} < \beta < 1$, we have $\lim_{h \to 0} \mathrm{Re}(\mu) = -\infty$. Hence, $\mu \to -\infty$, which is on the infinite negative real axis of the complex plane. If $\beta < \frac{1}{2}$, we have $\lim_{h \to 0} \mathrm{Re}(\mu) = 0$. Hence, we get $\mu \to 0$. $\quad\square$

Lemma 4.2. *Suppose that a linear multistep method (ρ, σ) is strongly $A(\theta)$-stable $(0 \leq \theta \leq \pi/2)$. Then there exist positive constants r, γ, C, such that $\forall \mu \in S_\theta \equiv \{z \in \bar{\mathbb{C}} | z = 0 \text{ or } z = \infty \text{ or } -\theta_1 \leq Arg\ z \leq \theta_1, 0 \leq \theta_1 < \theta\}$, we have*

$$\|R(\mu)^n\| \leq Ce^{-\gamma n}, \quad \text{if } |\mu| \geq r;$$
$$\|R(\mu)^n\| \leq Ce^{\gamma n Re(\mu)}, \quad \text{if } |\mu| \leq r.$$

Proof. See Lemma 3 in [9]. $\qquad\qquad\square$

Combining Lemmas 4.1 and 4.2, we see that when $\frac{1}{2} < \beta \leq \beta_{\max}$, we have $\|R(\mu)^n\| \leq Ce^{-\gamma n}$; and when $\beta < \frac{1}{2}$, we have $\|R(\mu)^n\| \leq Ce^{\gamma n Re(\mu)}$. For the case when $\beta = \frac{1}{2}$, we can see from the proof of Lemma 4.1 that $Re(\mu) \rightarrow -d$ and $|\mu| \rightarrow d$ as $h \rightarrow 0$. Thus, if $|\mu| \geq r$, we have $\|R(\mu)^n\| \leq Ce^{-\gamma n}$, and, if $|\mu| \leq r$, we have $\|R(\mu)^n\| \leq Ce^{-\gamma n d}$, which decays exponentially as well.

Lemma 4.3. *Let $\varepsilon^{(l)}$ be defined by (30), β as in (31), and μ as in (24). We have*

$$|\varepsilon^{(l)}| \leq \frac{12}{25}\left(\frac{20}{3}|z|^5 + |\mu + z||e^{-4z}|\right)|\hat{v}(t_l)|.$$

Proof. For notation convenience, we look at $\varepsilon^{(l-4)}$. We first note that

$$\hat{\alpha}_4 \varepsilon^{(l-4)} = \sum_{j=0}^{4} \hat{\alpha}_{4-j} \hat{v}(t_{l-j})$$

$$= \sum_{j=0}^{4} \alpha_{4-j} \hat{v}(t_{l-j}) + z\hat{v}(t_l) - (\mu + z)\hat{v}(t_l)$$

$$= \sum_{j=0}^{4} \alpha_{4-j} \hat{v}(t_{l-j}) - k\hat{V}_t(t_l) - (\mu + z)\hat{v}(t_l).$$

Applying Taylor expansion to $\hat{v}(t_{l-j})$ and get

$$\hat{v}(t_{l-j}) = \hat{v}(t_l) - jk\hat{V}_t(t_l) + \frac{j^2 k^2}{2}\hat{V}_{tt}(t_l) - \frac{j^3 k^3}{6}\hat{V}_{ttt}(t_l) + \frac{j^4 k^4}{24}\hat{V}_{tttt}(t_l) + \int_{t_l}^{t_{l-j}} \frac{(t_{l-j} - t)^4}{24}\hat{V}_{ttttt}(t)dt.$$

From the properties of BDF4 coefficients and the fact that $\hat{V}(t) = e^{-(\omega^2 + ia\omega)t}$ is infinitely smooth, we have

$$\sum_{j=0}^{4} \alpha_{4-j}\hat{v}(t_{l-j}) - k\hat{V}_t(t_l) = \frac{-(\omega^2 + ia\omega)^5}{24}\sum_{j=1}^{4} \alpha_{4-j}\int_{t_l}^{t_{l-j}}(t_{l-j} - t)^4 e^{-(\omega^2 + ia\omega)t}dt,$$

and

$$
\begin{aligned}
|\varepsilon^{(l-4)}| &= \left| \frac{1}{\alpha_4 - \mu} \left(\frac{-(\omega^2 + ia\omega)^5}{24} \sum_{j=1}^{4} \alpha_{4-j} \int_{t_l}^{t_{l-j}} (t_{l-j} - t)^4 e^{-(\omega^2 + ia\omega)t} dt - (\mu + z)\hat{v}(t_l) \right) \right| \\
&\leq \frac{1}{\alpha_4} \left(\frac{|\omega^2 + ia\omega|^5}{24} \left| \sum_{j=1}^{4} \alpha_{4-j} \int_{t_{l-j}}^{t_l} (t - t_{l-j})^4 e^{-(\omega^2 + ia\omega)t} dt \right| + |\mu + z||\hat{v}(t_l)| \right) \\
&\leq \frac{1}{\alpha_4} \left(\frac{|\omega^2 + ia\omega|^5}{24} \sum_{j=2,4} \alpha_{4-j} \left| \int_{t_{l-j}}^{t_l} (t - t_{l-j})^4 e^{-(\omega^2 + ia\omega)t} dt \right| + |\mu + z||\hat{v}(t_l)| \right) \\
&\leq \frac{1}{\alpha_4} \left(\frac{|\omega^2 + ia\omega|^5 k^4}{24} \sum_{j=2,4} \alpha_{4-j} j^4 \left| \int_{t_{l-j}}^{t_l} e^{-(\omega^2 + ia\omega)t} dt \right| + |\mu + z||\hat{v}(t_l)| \right) \\
&\leq \frac{1}{\alpha_4} \left(\frac{|\omega^2 + ia\omega|^5 k^4}{24} \sum_{j=2,4} \alpha_{4-j} j^4 \cdot jk \, |\hat{v}(t_{l-j})| + |\mu + z||e^{-(\omega^2 + ia\omega)4k} \hat{v}(t_{l-4})| \right) \\
&\leq \frac{1}{\alpha_4} \left(\frac{|\omega^2 + ia\omega|^5 k^5}{24} \sum_{j=2,4} \alpha_{4-j} j^5 + |\mu + z||e^{-(\omega^2 + ia\omega)4k}| \right) |\hat{v}(t_{l-4})| \\
&= \frac{12}{25} \left(\frac{20}{3} |z|^5 + |\mu + z||e^{-(\omega^2 + ia\omega)4k}| \right) |\hat{v}(t_{l-4})|.
\end{aligned}
$$

$\square$

Theorem 4.4. *For the iteration scheme (23), there exist some positive constants γ, C_1, C_2, C_3 such that*

$$
\begin{aligned}
|\hat{E}^{(n)}| \leq &\, C_1 e^{-\gamma n} \max_{0 \leq j \leq 3} |\hat{V}^{(0)}| \mathbb{1}_{\{\frac{1}{2} \leq \beta \leq \beta_{\max}\}} \\
&+ \left(C_2 e^{\gamma n Re(\mu)} \max_{0 \leq j \leq 3} |\hat{E}^{(j)}| + C_3 h^4 |\omega|^\chi |\nu|^{\bar{\gamma}(n-1)} |\hat{v}(0)| \right) \mathbb{1}_{\{\beta < \frac{1}{2}, \omega = 0\}},
\end{aligned}
\tag{32}
$$

for $n \geq 4$, where $\nu = e^{-(\omega^2 + ia\omega)k}$, $\bar{\gamma} = \max(\gamma, 1)$, and $\chi = 5(1 + H(\beta))$.

Proof. When $\frac{1}{2} \leq \beta \leq \beta_{\max}$, the exact solution $\hat{v}(t_n) = e^{-nz}\hat{v}(0)$ converges to 0 exponentially. Hence, from Lemma 4.2, we have

$$
|\hat{E}^{(n)}| \leq \|\bar{E}^{(n)}\| \approx \|R^n \bar{V}^{(0)}\| \leq \|R^n\| \cdot \|\bar{V}^{(0)}\| \leq C_1 e^{-\gamma n} \max_{0 \leq j \leq 3} |\hat{V}^{(0)}|.
$$

When $\beta < \frac{1}{2}$, we note that

$$
Re(\mu) = -\omega^2 k + \frac{d}{90} \omega^6 h^5 + \mathcal{O}(\omega^8 h^7),
$$

and

$$
\left| \frac{d}{90} \omega^6 h^5 + \mathcal{O}(\omega^8 h^7) \right| = \left| \frac{d}{90} h^{5-6\beta} + \mathcal{O}(h^{7-8\beta}) \right| \leq Ch^2
$$

for some positive constant C. Hence, with $0 \leq j \leq n - 1 \leq \frac{T}{k}$, we have

$$
\begin{aligned}
e^{\gamma j \mathrm{Re}(\mu)} &\leq e^{-\gamma j \omega^2 k} \cdot e^{\gamma j \left| \frac{d}{90} \omega^6 h^5 + \mathcal{O}(\omega^8 h^7) \right|} \\
&\leq e^{-\gamma j \omega^2 k} \cdot e^{\gamma j C h^2} \\
&\leq e^{-\gamma j \omega^2 k} (1 + C j h^2) \\
&= |\nu|^{\gamma j} (1 + C j h^2).
\end{aligned}
$$

Here and in the following, the constants C at each step are not necessarily the same. Moreover, recalling that $z = (\omega^2 + i a \omega) k$, we have

$$
|z| \leq \begin{cases} C \omega^2 h, & \beta \geq 0, \\ C |\omega| h, & \beta < 0, \end{cases} \quad \text{and} \quad |\mu + z| \leq \begin{cases} C \omega^6 h^5, & \beta \geq 0, \\ C |\omega|^5 h^5, & \beta < 0. \end{cases}
$$

From Lemmas 4.2 and 4.3, we have

$$
\begin{aligned}
|\hat{E}^{(n)}| &\leq \|\bar{E}^{(n)}\| = \left\| R^n \bar{E}^{(0)} + \sum_{j=0}^{n-1} R^j \bar{\varepsilon}^{(n-1-j)} \right\| \\
&\leq \|R^n\| \cdot \|\bar{E}^{(0)}\| + \sum_{j=0}^{n-1} \|R^j\| \cdot |\varepsilon^{(n-1-j)}| \\
&\leq C e^{\gamma n \mathrm{Re}(\mu)} \|\bar{E}^{(0)}\| + C \frac{12}{25} \left(\frac{20}{3} |z|^5 + |\mu + z| |e^{-4z}| \right) |\hat{v}(0)| \sum_{j=0}^{n-1} e^{\gamma j \mathrm{Re}(\mu)} |\nu|^{n-1-j} \\
&\leq C e^{\gamma n \mathrm{Re}(\mu)} \|\bar{E}^{(0)}\| + C \left(\frac{20}{3} |z|^5 + |\mu + z| \right) |\hat{v}(0)| \sum_{j=0}^{n-1} |\nu|^{\gamma j + n - 1 - j} (1 + C j h^2) \\
&\leq C e^{\gamma n \mathrm{Re}(\mu)} \|\bar{E}^{(0)}\| + C |\omega|^\chi h^5 |\hat{v}(0)| |\nu|^{\bar{\gamma}(n-1)} \sum_{j=0}^{n-1} (1 + C j h^2) \\
&\leq C e^{\gamma n \mathrm{Re}(\mu)} \|\bar{E}^{(0)}\| + C |\omega|^\chi h^5 |\hat{v}(0)| |\nu|^{\bar{\gamma}(n-1)} n \\
&\leq C e^{\gamma n \mathrm{Re}(\mu)} \max_{0 \leq j \leq 3} |\hat{E}^{(j)}| + C |\omega|^\chi h^5 |\hat{v}(0)| \frac{|\nu|^{\bar{\gamma}(n-1)}}{h} \\
&= C_2 e^{\gamma n \mathrm{Re}(\mu)} \max_{0 \leq j \leq 3} |\hat{E}^{(j)}| + C_3 h^4 |\omega|^\chi |\nu|^{\bar{\gamma}(n-1)} |\hat{v}(0)|.
\end{aligned}
$$

$\square$

Remark 4.1. *Theorem 4.4 shows that the high-frequency error of BDF4 decays exponentially, while the low-frequency error involves the error from the three steps of initialization, and a fourth-order component.*

Remark 4.2. *From the proof of Theorem 4.4, we see that, for $l \geq 4$, assuming $\hat{E}^{(l-j)} = 0$ for $j = 4, 3, 2, 1$,*

the error of BDF4 satisfies

$$
\begin{aligned}
|\hat{E}^{(l)}| \leq\ & C_1 e^{-\gamma} \max_{0\leq j\leq 3} |\hat{V}^{(0)}| \mathbb{1}_{\{\frac{1}{2}\leq\beta\leq\beta_{\max}\}} \\
& + \left(C_2 e^{\gamma Re(\mu)} \max_{0\leq j\leq 3} |\hat{E}^{(j)}| + C_3 h^5 |\omega|^{\chi} |\hat{v}(0)| \right) \mathbb{1}_{\{\beta<\frac{1}{2},\omega=0\}},
\end{aligned}
\tag{33}
$$

which is what we would expect for the local error.

Remark 4.3. *We study the convergence behavior with BDF4 time stepping in particular, but it is easy to see that the proof process does not rely on the order of the BDF method, and the conclusions can be similarly extended to other methods in the BDF family. For example, the frequency error applying BDF3 converges exponentially in the same high-frequency domain as BDF4, while it converges as $\mathcal{O}(h^3 |\omega|^{\chi} |\hat{v}(0)|)$ globally, and as $\mathcal{O}(h^4 |\omega|^{\chi} |\hat{v}(0)|)$ locally in the same low-frequency domain.*

5 Initializing BDF4

Third order methods are sufficient to initialize the first three time steps in order to obtain global fourth-order convergence with BDF4. For all the three different initial conditions, we carry the analysis of a classic third-order explicit Runge-Kutta method (RK3) to solve the first and second time steps, and a third order backward differential formula to solve the third time step. BDF3 for solving the third time step follows the update rule

$$
\frac{\frac{11}{6} V_j^{(3)} - 3 V_j^{(2)} + \frac{3}{2} V_j^{(1)} - \frac{1}{3} V_j^{(0)}}{k} = \mathcal{D}_h V_j^{(3)}.
\tag{34}
$$

We have already studies the convergence behavior of BDF methods.

The RK3 used in the first two steps is given by the Butcher tableau

$$
\begin{array}{c|ccc}
0 & 0 & 0 & 0 \\
1/2 & 1/2 & 0 & 0 \\
1 & -1 & 2 & 0 \\
\hline
& 1/6 & 2/3 & 1/6
\end{array}
$$

We study its convergence in the following subsection.

5.1 Fourier analysis of RK3 applied to nonsmooth data

Recall that the semi-discrete ODE system we are solving is $\frac{dV_j}{dt} = \mathcal{D}_h V_j$. Without loss of generality, we consider applying RK3 to the first time step and compute the solution at x_j by computing

$$f_1 = \mathcal{D}_h V_j^{(0)},$$
$$f_2 = \mathcal{D}_h \left(V_j^{(0)} + \frac{k}{2} f_1 \right)$$
$$f_3 = \mathcal{D}_h (V_j^{(0)} - k f_1 + 2k f_2),$$

and

$$V_j^{(1)} = V_j^{(0)} + \frac{k}{6}(f_1 + 4f_2 + f_3) = V_j^{(0)} + k\mathcal{D}_h V_j^{(0)} + \frac{k^2}{2}\mathcal{D}_h^2 V_j^{(0)} + \frac{k^3}{6}\mathcal{D}_h^3 V_j^{(0)}.$$

Defining the operator

$$\mathcal{K}_{k,h} \equiv 1 + k\mathcal{D}_h + \frac{k^2}{2}\mathcal{D}_h^2 + \frac{k^3}{6}\mathcal{D}_h^3,$$

one step of RK3 is simply

$$V_j^{(1)} = \mathcal{K}_{k,h} V_j^{(0)}. \tag{35}$$

We see that $\mathcal{K}_{k,h} V_j^{(0)}$ is similar to a truncated Taylor expansion of $v(k, x_j)$ around $t = 0$ with the time derivatives $\dot{v}(0, x_j), \ddot{v}(0, x_j)$ and $\dddot{v}(0, x_j)$ being replaced by $\mathcal{D}_h V_j^{(0)}, \mathcal{D}_h^2 V_j^{(0)}$ and $\mathcal{D}_h^3 V_j^{(0)}$, respectively. If the initial data $V^{(0)}$ were smooth enough in space, since $\frac{\partial v}{\partial t} = \frac{\partial^2 v}{\partial x^2} - a\frac{\partial v}{\partial x}$, then $\mathcal{D}_h V_j^{(0)}, \mathcal{D}_h^2 V_j^{(0)}$ and $\mathcal{D}_h^3 V_j^{(0)}$ would simply be the fourth-order FD approximations of $\dot{v}(0, x_j), \ddot{v}(0, x_j)$ and $\dddot{v}(0, x_j)$, respectively. Hence, $V_j^{(1)} = \mathcal{K}_{k,h} V_j^{(0)}$ would be a fourth-order approximation of first time step solution $v(k, x_j)$.

For nonsmooth initial conditions, the convergence order analysis is more involved. We study this through the analysis of the Fourier transform of $\mathcal{K}_{k,h}$. The Fourier transform of $\mathcal{D}_h$ is

$$\mathcal{F}[\mathcal{D}_h](\omega) = \mathcal{F}[\mathcal{D}_h](\theta/\pi) = -\frac{\cos(2\theta) - 16\cos\theta + 15}{6h^2} - ia\frac{8\sin\theta - \sin(2\theta)}{6h}.$$

To derive $\mathcal{F}(\mathcal{D}_h^2)$ and $\mathcal{F}(\mathcal{D}_h^3)$, we note that $\mathcal{D}_h = D_4^2 - aD_4$, $\mathcal{D}_h^2 = D_4^4 - aD_4^2 D_4 - aD_4 D_4^2 + a^2 D_4 D_4$, and $\mathcal{D}_h^3 = D_4^6 - a(D_4^4 D_4 + D_4^2 D_4 D_4^2 + D_4 D_4^4) + a^2(D_4^2 D_4 D_4 + D_4 D_4^2 D_4 + D_4 D_4 D_4^2) - a^3 D_4 D_4 D_4$, which give

$$\mathcal{D}_h^2 V_j = \left(\frac{1}{h^4}D^{(2,0)} - a\frac{1}{h^3}D^{(2,1)} + a^2\frac{1}{h^2}D^{(2,2)} \right)^T V_{j-4:j+4},$$

and

$$\mathcal{D}_h^3 V_j = \left(\frac{1}{h^6}D^{(3,0)} - a\frac{1}{h^5}D^{(3,1)} + a^2\frac{1}{h^4}D^{(3,2)} - a^3\frac{1}{h^3}D^{(3,3)} \right)^T V_{j-6:j+6},$$

where $D^{(i,j)}$ are column vectors with entries given in the tables

$D^{(2,0)}$	$\frac{1}{144}$	$\frac{-32}{144}$	$\frac{316}{144}$	$\frac{-992}{144}$	$\frac{1414}{144}$	$\frac{-992}{144}$	$\frac{316}{144}$	$\frac{-32}{144}$	$\frac{1}{144}$
$D^{(2,1)}$	$\frac{-1}{72}$	$\frac{24}{72}$	$\frac{-158}{72}$	$\frac{248}{72}$	0	$\frac{-248}{72}$	$\frac{158}{72}$	$\frac{-24}{72}$	$\frac{1}{72}$
$D^{(2,2)}$	$\frac{1}{144}$	$\frac{-16}{144}$	$\frac{64}{144}$	$\frac{16}{144}$	$\frac{-130}{144}$	$\frac{16}{144}$	$\frac{64}{144}$	$\frac{-16}{144}$	$\frac{1}{144}$

and

$D^{(3,0)}$	$\frac{-1}{1728}$	$\frac{48}{1728}$	$\frac{-858}{1728}$	$\frac{7024}{1728}$	$\frac{-27279}{1728}$	$\frac{58464}{1728}$	$\frac{-74796}{1728}$	$\frac{58464}{1728}$	$\frac{-27292}{1728}$	$\frac{7024}{1728}$	$\frac{-858}{1728}$	$\frac{48}{1728}$	$\frac{-1}{1728}$
$D^{(3,1)}$	$\frac{1}{576}$	$\frac{-40}{576}$	$\frac{572}{576}$	$\frac{-3512}{576}$	$\frac{9093}{576}$	$\frac{-9744}{576}$	0	$\frac{9744}{576}$	$\frac{-9093}{576}$	$\frac{3512}{576}$	$\frac{-572}{576}$	$\frac{40}{576}$	$\frac{-1}{576}$
$D^{(3,2)}$	$\frac{-1}{576}$	$\frac{32}{576}$	$\frac{-350}{576}$	$\frac{1504}{576}$	$\frac{-1791}{576}$	$\frac{-1536}{576}$	$\frac{4284}{576}$	$\frac{-1536}{576}$	$\frac{-1791}{576}$	$\frac{1504}{576}$	$\frac{-350}{576}$	$\frac{32}{576}$	$\frac{-1}{576}$
$D^{(3,3)}$	$\frac{1}{1728}$	$\frac{-24}{1728}$	$\frac{192}{1728}$	$\frac{-488}{1728}$	$\frac{-387}{1728}$	$\frac{1584}{1728}$	0	$\frac{-1584}{1728}$	$\frac{387}{1728}$	$\frac{499}{1728}$	$\frac{-192}{1728}$	$\frac{24}{1728}$	$\frac{-1}{1728}$

and the notation $V_{j_1:j_2}$ is borrowed from Matlab. Therefore, we get (including $\mathcal{F}[\mathcal{D}_h](\omega)$ derived before)

$$\mathcal{F}[\mathcal{D}_h](\omega) = -\frac{\cos(2\theta) - 16\cos\theta + 15}{6h^2} - ia\frac{8\sin\theta - \sin(2\theta)}{6h},$$

$$\mathcal{F}[\mathcal{D}_h^2](\omega) = \frac{707 + \cos(4\theta) - 32\cos(3\theta) + 316\cos(2\theta) - 992\cos\theta}{72h^4}$$
$$+ a^2\frac{-65 + \cos(4\theta) - 16\cos(3\theta) + 64\cos(2\theta) + 16\cos\theta}{72h^2}$$
$$- ia\frac{\sin(4\theta) - 24\sin(3\theta) + 158\sin(2\theta) - 248\sin\theta}{36h^3},$$

$$\mathcal{F}[\mathcal{D}_h^3](\omega) = \frac{-37398 - \cos(6\theta) + 48\cos(5\theta) - 858\cos(4\theta) + 7024\cos(3\theta) - 27279\cos(2\theta) + 58464\cos\theta}{864h^6}$$
$$+ a^2\frac{2142 - \cos(6\theta) + 32\cos(5\theta) - 350\cos(4\theta) + 1504\cos(3\theta) - 1791\cos(2\theta) - 1536\cos\theta}{288h^4}$$
$$- ia\frac{-\sin(6\theta) + 40\sin(5\theta) - 572\sin(4\theta) + 3512\sin(3\theta) - 9093\sin(2\theta) + 9744\sin\theta}{288h^5}$$
$$- ia^3\frac{-\sin(6\theta) + 24\sin(5\theta) - 192\sin(4\theta) + 488\sin(3\theta) + 387\sin(2\theta) - 1584\sin\theta}{864h^3},$$

where we recall $\theta = \omega h$. The RK3 iteration for the first time step in the frequency domain is

$$\hat{V}^{(1)}(\omega) = \left(1 + k\mathcal{F}[\mathcal{D}_h](\omega) + \frac{k^2}{2}\mathcal{F}[\mathcal{D}_h^2](\omega) + \frac{k^3}{6}\mathcal{F}[\mathcal{D}_h^3](\omega)\right)\hat{V}^{(0)}(\omega).$$

Similar to the discussion in the previous section, we study the convergence of one RK3 iteration for different magnitudes of ω with respect to h. Applying Maclaurin series expansion to $\mathcal{F}[\mathcal{D}_h](\omega)$, $\mathcal{F}[\mathcal{D}_h^2](\omega)$ and

$F[\mathcal{D}_h^3](\omega)$, we have

$$\mathcal{F}[\mathcal{D}_h](\omega) = -(\omega^2 + ia\omega) + \frac{1}{90}(\omega^6 + i3a\omega^5)h^4 + \cdots,$$

$$\mathcal{F}[\mathcal{D}_h^2](\omega) = (\omega^4 - \frac{1}{45}\omega^8 h^4 + \cdots) - a^2(\omega^2 - \frac{1}{15}\omega^6 h^4 + \cdots) - ia(-2\omega^3 + \frac{4}{45}\omega^7 h^4 + \cdots)$$

$$= (\omega^2 + ia\omega)^2 + \frac{1}{45}(-\omega^8 + 3a^2\omega^6 - i4a\omega^7)h^4 + \cdots,$$

$$\mathcal{F}[\mathcal{D}_h^3](\omega) = (-\omega^6 + \frac{1}{30}\omega^{10}h^4 + \cdots) + a^2(3\omega^4 - \frac{7}{30}\omega^8 h^4 + \cdots)$$

$$- ia(3\omega^5 - \frac{1}{6}\omega^9 h^4 + \cdots) + ia^3(\omega^3 - \frac{1}{10}\omega^7 h^4 + \cdots)$$

$$= -(\omega^2 + iaw)^3 + \frac{1}{30}(\omega^{10} - 7a^2\omega^8 + i5a\omega^9 - i3a^3\omega^7)h^4 + \cdots.$$

The results match our expectation by noticing that the exact frequency satisfies

$$\frac{\partial^n}{\partial t^n}\hat{v}(t,\omega) = (-1)^n(\omega^2 + ia\omega)^n \hat{v}(t,\omega),$$

and

$$\hat{v}(t_1,\omega) = e^{-(\omega^2 + ia\omega)k}\hat{V}(t_0,\omega)$$

$$= \left(1 - (\omega^2 + ia\omega)k + \frac{k^2}{2}(\omega^2 + ia\omega)^2 - \frac{k^3}{6}(\omega^2 + ia\omega)^3 + \ldots\right)\hat{v}(t_0,\omega).$$

Given $\hat{V}^{(0)}(\omega) = \hat{v}(t_0,\omega) + \hat{E}^{(0)}(\omega)$, where $\hat{E}^{(0)}$ is the frequency error at the initial time step, which is intrinsic to the initial condition discretization, we see that the error in $\hat{V}^{(1)}$ from one RK3 iteration is simply

$$\hat{E}^{(1)} = \hat{V}^{(1)} - \hat{v}(t_1)$$

$$= \left(1 + k\mathcal{F}[\mathcal{D}_h](\omega) + \frac{k^2}{2}\mathcal{F}[\mathcal{D}_h^2](\omega) + \frac{k^3}{6}\mathcal{F}[\mathcal{D}_h^3](\omega)\right)\hat{E}^{(0)} + (-1)^{j+1}\sum_{j=4}^{\infty}\frac{(\omega^2 k + ia\omega k)^j}{j!}\hat{v}(t_0)$$

$$+ \left\{\frac{1}{90}\left((\omega^6 + i3a\omega^5)k + (-\omega^8 + 3a^2\omega^6 - i4a\omega^7)k^2 + \frac{1}{2}(\omega^{10} - 7a^2\omega^8 + i5a\omega^9 - i3a^3\omega^7)k^3\right)h^4 + \cdots\right\}\hat{v}(t_0).$$

(36)

The error behaves differently in the high- and low-frequency regimes. We discuss this below. Recall that $k = dh \sim h$.

1. First consider the case $\omega = h^{-\beta}$ with $\beta < \frac{1}{2}$, i.e. $\omega^2 h \to 0$ as $h \to 0$. We see from (36) that the error $\hat{E}^{(1)}$ from one step of RK3 is comprised of $\hat{E}^{(0)}$ multiplied by a constant order coefficient, plus the remaining $\mathcal{O}(z^4)$ terms. Therefore, we have

$$|\hat{V}^{(1)} - \hat{v}(t_1)| \leq C_1'|\hat{E}^{(0)}| + C_2'|z|^4|\hat{v}(t_0)|,$$

(37)

where C_i' and C_2' are some positive constants. Since $\hat{E}^{(0)}$ is multiplied by a constant order coefficient, it cannot be reduced by RK3 time stepping. This explains why smoothing is necessary so that $\hat{E}^{(0)}$ is of high order as well.

2. Consider $\omega = h^{-\beta}$ with $\frac{1}{2} \le \beta \le \beta_{\max}$, i.e. $\omega^2 h \nrightarrow 0$ as $h \to 0$. Hence, we see from (36) that the error $\hat{V}^{(1)} - \hat{v}(t_1) \nrightarrow 0$ as $h \to 0$. Therefore, RK3 time stepping is not convergent in the high-frequency region $\omega = h^{-\beta}$ with $\frac{1}{2} \le \beta \le \beta_{\max}$, which lies exactly in the high-frequency exponential damping region of BDF4 scheme starting from the fourth time step, see Equation (32). As a result, even though RK3 is not convergent in a single time step in the high-frequency domain, the combination of RK3 as the initialization scheme and BDF4 for the general steps gives the expected $\mathcal{O}(z^4)$ order of convergence.

Therefore, in summary, RK3 time stepping gives

$$|\hat{E}^{(n)}| \le (\text{nonconvergent error}) \cdot \mathbb{1}_{\{\frac{1}{2} \le \beta \le \beta_{\max}\}} + \left(C_1'|\hat{E}^{(n-1)}| + C_2'|z|^4|\hat{v}(t_{n-1})| \right) \mathbb{1}_{\{\beta < \frac{1}{2}, \omega = 0\}}. \quad (38)$$

Remark 5.1. *Relation (38) shows that the high-frequency error of RK3 is not convergent, while the low-frequency error involves the error from the previous step and a fourth-order component. Combining RK3 and BDF4 (or any BDF method), the nonconvergent error of RK3 in the high-frequency domain is damped exponentially by BDF.*

In the low-frequency region, given $\hat{E}^{(0)}$, with two steps of RK3 initialization scheme, we have

$$|\hat{E}^{(1)}| \le C_1'|\hat{E}^{(0)}| + C_2'|z|^4|\hat{v}(t_0)|,$$
$$|\hat{E}^{(2)}| \le C_1'|\hat{E}^{(1)}| + C_2'|z|^4|\hat{v}(t_1)| \le C_3'|\hat{E}^{(0)}| + |z|^4(C_4'|\hat{v}(t_0)| + C_5'|\hat{v}(t_1)|),$$

where C_i' for $i = 1, \ldots, 5$ are positive constants. Note that the final convergence behavior is determined by the accuracy of $\hat{E}^{(0)}$, which also needs to be of high order. We discuss this in the next section.

6   High-order smoothing of the initial conditions

Due to the nonsmoothness in the Dirac delta, Heaviside and ramp initial conditions, to achieve global fourth-order convergence, we still need to make sure that the initial condition is discretized to a high-order in the frequency domain. In this paper, we perform initial condition smoothing using the smoothing operator suggested in [8]. In particular, a fourth-order smoothing operator Φ_4 is given by the inverse Fourier transform of

$$\hat{\Phi}_4(\omega) = \left(\frac{\sin(\omega/2)}{\omega/2} \right)^4 \left[1 + \frac{2}{3}\sin^2(\omega/2) \right].$$

The smoothed initial condition is then computed from

$$\tilde{v}_{Kreiss}^{(0)}(x) = \frac{1}{h} \int_{-3h}^{3h} \Phi_4(s/h) v(t_0, x - s) ds. \quad (39)$$

$V_j^{(0)}$	Dirac delta	Heaviside	Ramp
$j < -3$	0	0	0
$j = -3$	$\frac{(\alpha-1)^3}{36h}$	$-\frac{(\alpha-1)^4}{144}$	$\frac{(\alpha-1)^5 h}{720}$
$j = -2$	$-\frac{(11\alpha^3-30\alpha^2+24\alpha-4)}{36h}$	$\frac{(11\alpha^4-40\alpha^3+48\alpha^2-16-4)}{144}$	$\frac{(-11\alpha^5+50\alpha^4-80\alpha^3+40\alpha^2+20\alpha-20)h}{720}$
$j = -1$	$\frac{(14\alpha^3-27\alpha^2+15)}{18h}$	$\frac{(-7\alpha^4+18\alpha^3-30\alpha+18)}{36}$	$\frac{(14\alpha^5-45\alpha^4+150\alpha^2-180\alpha+51)h}{360}$
$j = 0$	$\frac{(-14\alpha^3+15\alpha^2+12\alpha+2)}{18h}$	$\frac{(7\alpha^4-10\alpha^3-12\alpha^2-4\alpha+37)}{36}$	$-\frac{(14\alpha^5-25\alpha^4-40\alpha^3-20\alpha^2+370\alpha-350)h}{360}$
$j = 1$	$-\frac{(-11\alpha^3+3\alpha^2+3\alpha+1)}{36h}$	$\frac{(-11\alpha^4+4\alpha^3+6\alpha^2+4\alpha+145)}{144}$	$-\frac{(-11\alpha^5+5\alpha^4+10\alpha^3+10\alpha^2+725\alpha-1439)h}{720}$
$j = 2$	$-\frac{\alpha^3}{36h}$	$\frac{\alpha^4+144}{144}$	$-\frac{(\alpha^5+720\alpha-2160)h}{720}$
$j > 2$	0	1	$(j+1-\alpha)h$

Table 1: Fourth-order smoothed discrete Dirac delta, Heaviside and ramp initial conditions

We calculated explicit formulas for the fourth-order discrete Dirac delta, Heaviside and ramp initial conditions arising after applying the smoothing operator (39), and present them in Table 1. Using the smoothed initial condition discretizations given in Table 1, we guarantee that the initial conditions are fourth-order accurate in the frequency domain, and hence, $\hat{E}^{(0)} = \mathcal{O}(|\omega|^p h^4)$ for some positive constant p. Note that an appropriate linear combination of the smoothed ramp functions gives us the smoothed discretization of the bump function.

7 Solution error analysis

Now that we have analyzed the solution behavior in the Fourier frequency domain, we can perform inverse Fourier transform to recover the actual solution error. For the Dirac delta initial condition, we have

$$E^{(n)}(x_j) = \frac{1}{2\pi}\int_{-\frac{\pi}{h}}^{\frac{\pi}{h}} \hat{E}^{(n)}(\omega)e^{i\omega x_j}\,d\omega$$

$$\leq \frac{1}{2\pi}\int_{-\frac{\pi}{h}}^{\frac{\pi}{h}} C_1 e^{-\gamma n}\max_{0\leq j\leq 3}|\hat{V}^{(0)}|\mathbb{1}_{\{\frac{1}{2}\leq\beta\leq\beta_{\max}\}}e^{i\omega x_j}\,d\omega$$

$$+\frac{1}{2\pi}\int_{-\frac{\pi}{h}}^{\frac{\pi}{h}}\left(C_2 e^{\gamma n\mathrm{Re}(\mu)}\max_{0\leq j\leq 3}|\hat{E}^{(j)}| + C_3 h^4|\omega|^\chi|\nu|^{\bar{\gamma}(n-1)}|\hat{V}(0)|\right)\mathbb{1}_{\{\beta<\frac{1}{2},\omega=0\}}e^{i\omega x_j}\,d\omega$$

$$=C_1 e^{-\gamma n}\frac{\cos(\pi x_j/h)-\cos(x_j/\sqrt{h})}{i\pi x_j}\max_{0\leq j\leq 3}|\hat{V}^{(0)}|$$

$$+C_2\frac{1}{2\pi}\int_{-\sqrt{\frac{1}{h}}}^{\sqrt{\frac{1}{h}}}e^{\gamma n\mathrm{Re}(\mu)}\max_{0\leq j\leq 3}|\hat{E}^{(j)}|e^{i\omega x_j}\,d\omega + C_3\frac{1}{2\pi}\int_{-\sqrt{\frac{1}{h}}}^{\sqrt{\frac{1}{h}}}h^4|\omega|^\chi|\nu|^{\bar{\gamma}(n-1)}|\hat{V}(0)|e^{i\omega x_j}\,d\omega$$

$$\leq C_1 e^{-\gamma n}\max_{0\leq j\leq 3}|\hat{V}^{(0)}| + C_2 h^4\int_{-\sqrt{\frac{1}{h}}}^{\sqrt{\frac{1}{h}}}|\omega|^p e^{\gamma n\mathrm{Re}(\mu)}e^{i\omega x_j}\,d\omega + C_3 h^4|\hat{V}(0)|\int_{-\sqrt{\frac{1}{h}}}^{\sqrt{\frac{1}{h}}}|\omega|^\chi e^{-\bar{\gamma}\omega^2(n-1)k}e^{i\omega x_j}\,d\omega$$

$$\approx C_1 e^{-\gamma n}\max_{0\leq j\leq 3}|\hat{V}^{(0)}| + \left(C_2\int_{-\infty}^{\infty}|\omega|^p e^{\gamma n\mathrm{Re}(\mu)}e^{i\omega x_j}\,d\omega + C_3|\hat{V}(0)|\int_{-\infty}^{\infty}|\omega|^\chi e^{-\bar{\gamma}\omega^2(n-1)k}e^{i\omega x_j}\,d\omega\right)h^4$$

$$\leq C_1 e^{-\gamma n}\max_{0\leq j\leq 3}|\hat{V}^{(0)}| + (C_2 + C_3|\hat{V}(0)|)h^4,$$

where the constants C_j with the same index are not necessarily equal. From the derivation, we see that fourth-order convergence is obtained if the discretized initial condition is smoothed to fourth-order. For the Heaviside and ramp initial conditions, a minor difference is that inverse Fourier transform does not directly give the solution. Instead, we have

$$e^{-\eta x_j}E^{(n)}(x_j) = \frac{1}{2\pi}\int_{-\frac{\pi}{h}}^{\frac{\pi}{h}}\hat{E}^{(n)}(\omega)e^{i\omega x_j}\,d\omega,$$

which gives

$$E^{(n)}(x_j) \leq e^{\eta x_j}C_1 e^{-\gamma n}\max_{0\leq j\leq 3}|\hat{V}^{(0)}| + e^{\eta x_j}(C_2 + C_3|\hat{V}(0)|)h^4.$$

8 Numerical results

8.1 Solving the model PDE

In this section, we provide numerical results to demonstrate the fourth-order convergence of our methods for solving the model problem (2) with nonsmooth initial conditions (3), (4), (5), and (12). We consider a truncated space domain on $x \in [-4, 4]$, with exact Dirichlet boundary conditions. Although our convergence study relies on Fourier analysis which assumes $x \in (-\infty, \infty)$, it turns out the conclusions we obtained still hold on the truncated domain with exact boundary conditions.

    In practice, it may be inconvenient to maintain the grid alignment value α to a fixed number. For this

reason, we consider cases where the grid alignment changes for each refinement, by slightly shifting the nonsmooth point to $x = 0.123$ while keeping the space domain $x \in [-4, 4]$ unchanged. We apply the fourth-order smoothed initial condition discretizations given in Table 1, for the Dirac delta, Heaviside and ramp initial conditions, respectively, with $a = 2, T = 1$. To also verify the correctness of our convergence analysis on the effect of smoothed and unsmoothed initial data, we show convergence results both with and without the smoothing of initial conditions. Tables 2, 3 and 4 show that directly applying the discrete initial conditions (14), (15) and (16) leads to low-order and inconsistent convergence, while with the smoothing modifications, we restore stable fourth-order convergence. We have also listed in the tables the convergence results of the solution derivatives. The results clearly show stable fourth-order accuracy.

To demonstrate the intrinsic high-frequency damping properties of BDF time stepping, we solve the model convection-diffusion Equation (2) under the delta and Heaviside initial conditions with our RK3-BDF3-BDF4 method and with the Crank-Nicolson (CN) method, respectively, and compare the solutions. We apply the same fourth-order FD discretization in space, and the original initial condition discretizations given by (14), (15) without any smoothing modifications to make sure we are only looking at the effect of different time-stepping schemes. Figure 2 shows comparisons between the numerical solutions to the model problem with $a = 2$ and $T = 0.1$. We choose $h = 0.0211$, $d = \frac{k}{h} = 0.1185$ for solving the PDE with delta initial condition, and $h = 0.0123$, $d = \frac{k}{h} = 0.2033$ for the Heaviside initial condition. As seen in Figure 2, CN time stepping by itself fails to converge in L_∞, and generates oscillatory solutions. After replacing the first two steps of CN approximation by four half-timestep backward Euler time marching (CN-Rannacher), the oscillations disappear [7]. On the other hand, due to the high-frequency damping property of BDF4, we observe that no spurious oscillations occur in the solutions and solution derivatives with the RK3-BDF3-BDF4 method.

Finally, to show that our method can be applied to solve PDEs with more complicated nonsmooth initial conditions constructed from the three basic nonsmooth functions, in Table 5, we present convergence results for solving the model PDE with the bump initial condition (12). In this table, we list the maximum error across all gridpoints (as an approximation to the ∞-norm of the error). The results clearly demonstrate fourth-order convergence of the solution, with slight degeneration in the solution derivatives.

8.2 Application to option pricing

In this section, we apply our algorithm to compute the Black-Scholes PDE (1) for option pricing problems. Although one can convert (1) to constant-coefficients PDE, we apply our methods to the original Black-Scholes PDE (1). As will be seen, the numerical results agree with our analysis shown for the model PDE (2). We consider three types of European options: digital call, call and a butterfly spread, corresponding to the Heaviside, ramp and bump initial conditions we discussed for the model PDE. The payoff function for a digital call with strike K is the shifted Heaviside function

$$G_D(T) = H(S - K).$$

The payoff function for a call option with strike K is the shifted ramp function

$$G_C(T) = \max(S - K, 0).$$
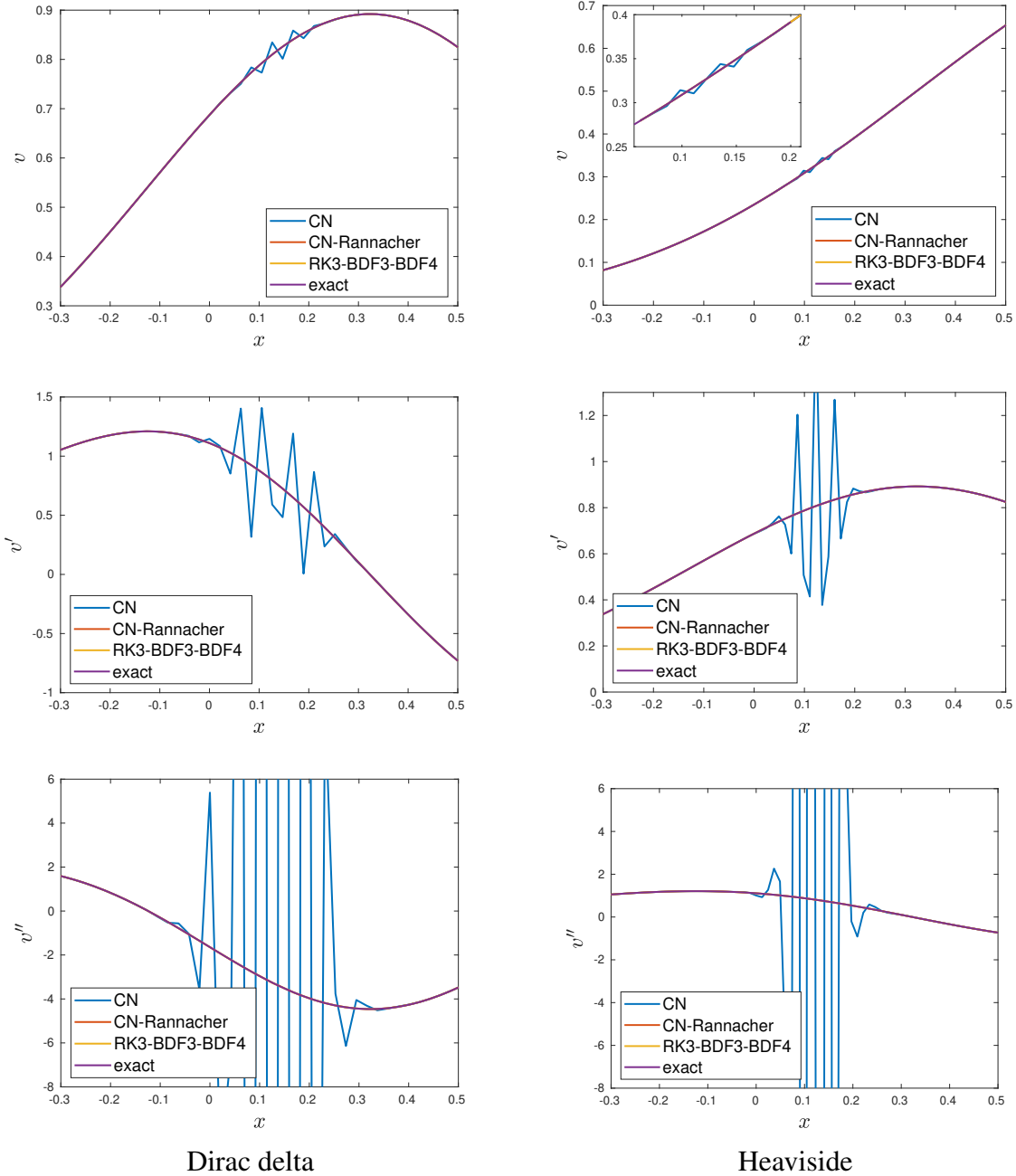
Figure 2: Comparison of numerical solutions and the calculated derivatives around the nonsmooth point from solving the model PDE (2) with $a = 2$ using CN, CN-Rannacher and RK3-BDF3-BDF4 time stepping.

A butterfly spread is a combination of four options: two long position calls struck at $K_1 = K - \mathcal{B}$ and $K_3 = K + \mathcal{B}$, and two short position calls struck at $K_2 = K$, where $\mathcal{B} > 0$ is given. The payoff function is a linear combination of the ramp functions

$$G_B(T) = \max(S - K_1, 0) - 2\max(S - K_2, 0) + \max(S - K_3, 0).$$

N	α	v			v'		v''	
		value	error	conv	error	conv	error	conv
				w/o smoothing				
20	0.3075	0.1045846	8.12e-04	-	3.27e-04	-	1.37e-03	-
40	0.6150	0.1040104	2.33e-04	1.80	2.30e-04	0.50	5.67e-04	1.27
80	0.2300	0.1038231	4.62e-05	2.33	4.23e-05	2.45	1.11e-04	2.35
160	0.4600	0.1037930	1.61e-05	1.52	1.60e-05	1.41	4.01e-05	1.47
320	0.9200	0.1037781	1.18e-06	3.77	1.21e-06	3.72	2.98e-06	3.75
				w smoothing				
20	0.3075	0.103747622	8.13e-05	-	4.28e-04	-	9.05e-04	-
40	0.6150	0.103775024	1.36e-06	5.90	2.67e-05	4.00	3.47e-05	4.70
80	0.2300	0.103776728	1.53e-07	3.15	1.69e-06	3.98	2.19e-06	3.99
160	0.4600	0.103776867	9.42e-09	4.02	1.06e-07	3.99	1.34e-07	4.03
320	0.9200	0.103776874	7.06e-10	3.74	6.60e-09	4.01	8.66e-09	3.96

Table 2: Convergence results at the nonsmooth point $x = 0.123$, $T = 1$, for solving the model problem (2) with the *Dirac delta initial condition*, taking $a = 2$. The grid alignment value α is different on each grid refinement level as given in the table, and the number of space intervals $M = N$.

N	α	v			v'		v''	
		value	error	conv	error	conv	error	conv
				w/o smoothing				
20	0.3075	0.0700980	8.56e-03	-	8.26e-03	-	3.46e-03	-
40	0.6150	0.0808755	2.23e-03	1.94	2.31e-03	1.84	1.30e-03	1.41
80	0.2300	0.0758418	2.81e-03	-0.34	2.81e-03	-0.28	1.40e-03	-0.11
160	0.4600	0.0784314	2.18e-04	3.69	2.13e-04	3.72	9.84e-05	3.83
320	0.9200	0.0797423	1.09e-03	-2.32	1.09e-03	-2.36	5.43e-04	-2.47
				w smoothing				
20	0.3075	0.078481631	1.73e-04	-	5.83e-05	-	4.11e-04	-
40	0.6150	0.078638802	1.10e-05	3.98	3.94e-06	3.89	2.59e-05	3.99
80	0.2300	0.078648921	6.90e-07	3.99	2.70e-07	3.87	1.63e-06	3.99
160	0.4600	0.078649561	4.33e-08	4.00	1.68e-08	4.01	1.02e-07	4.00
320	0.9200	0.078649601	2.71e-09	4.00	1.05e-09	4.00	6.40e-09	4.00

Table 3: Convergence results at the nonsmooth point $x = 0.123$, $T = 1$, for solving the model problem (2) with the *Heaviside initial condition*, taking $a = 2$. The grid alignment value α is different on each grid refinement level as given in the table, and the number of space intervals $M = N$

The parameters we use in the numerical experiments are: strike $K = 100$, $\mathcal{B} = 19.75$, expiry time $T = 0.5$, interest rate $r = 2\%$, zero dividend. The volatility σ is either 0.2 or 0.8 as given in the tables and figures. The semi-infinite spatial domain is truncated to $(0, S_b)$ with $S_b = 6K$, and exact Dirichlet conditions are applied.

Tables 6, 7 and 8 show the results of solving digital call, call and butterfly spread options, respectively, with variable α. We also list the convergence of the options' Δ and Γ at the single strike K for the

N	α	v			v'		v''	
		value	error	conv	error	conv	error	conv
				w/o smoothing				
20	0.3075	0.0504901	2.38e-04	-	1.74e-04	-	1.50e-04	-
40	0.6150	0.0504040	1.50e-04	0.67	1.39e-04	0.33	6.34e-05	1.24
80	0.2300	0.0502581	3.56e-06	5.39	3.92e-06	5.15	3.13e-06	4.34
160	0.4600	0.0502651	1.05e-05	-1.57	1.05e-05	-1.43	5.30e-06	-0.76
320	0.9200	0.0502515	3.00e-06	1.81	3.01e-06	1.81	1.52e-06	1.80
				w smoothing				
20	0.3075	0.050162772	9.04e-05	-	1.28e-04	-	5.99e-05	-
40	0.6150	0.050248754	5.58e-06	4.02	8.18e-06	3.96	1.56e-06	5.26
80	0.2300	0.050254186	3.49e-07	4.00	5.18e-07	3.98	4.87e-08	5.00
160	0.4600	0.050254519	2.18e-08	4.00	3.24e-08	4.00	1.85e-09	4.72
320	0.9200	0.050254540	1.36e-09	4.00	2.03e-09	4.00	6.76e-11	4.77

Table 4: Convergence results at the nonsmooth point $x = 0.123$, $T = 1$, for solving the model problem (2) with the *ramp initial condition*, taking $a = 2$. The grid alignment value α is different on each grid refinement level as given in the table, and the number of space intervals $M = N$.

N	α	v		v'		v''	
		max error	conv	max error	conv	max error	conv
			w/o smoothing				
20	0.3075	4.10e-03	-	1.78e-03	-	3.24e-03	-
40	0.6150	1.48e-03	1.47	7.31e-04	1.28	5.21e-04	2.64
80	0.2300	2.03e-04	2.87	1.27e-04	2.52	2.78e-04	0.91
160	0.4600	1.02e-04	0.99	1.32e-04	-0.06	2.51e-04	0.15
320	0.9200	1.30e-05	2.97	2.41e-05	2.46	4.73e-05	2.41
			w smoothing				
20	0.3075	1.35e-03	-	9.93e-04	-	2.16e-03	-
40	0.6150	8.81e-05	3.93	1.06e-04	3.23	3.06e-04	2.81
80	0.2300	5.48e-06	4.01	9.70e-06	3.45	2.57e-05	3.58
160	0.4600	3.41e-07	4.01	8.12e-07	3.58	1.97e-06	3.70
320	0.9200	2.18e-08	3.96	6.94e-08	3.55	1.58e-07	3.64

Table 5: Convergence results for maximum error and first and second derivatives, when solving the model problem (2) with the *bump initial condition* of spread $\mathcal{B}$, taking $a = 2$, $T = 1$. There are three nonsmooth points at $K - \mathcal{B}$, K, and $K + \mathcal{B}$, with $K = 0.123$, $\mathcal{B} = 1.321$. The grid alignment value α is different on each grid refinement level as given in the table, and the number of space intervals $M = N$.

digital call and call options, and at all the three kink points of the butterfly spread payoff function. In all experiments, fourth-order convergence is obtained for the option prices and calculated Δ and Γ applying our time-stepping scheme with smoothed initial conditions.

Again, we compare the solutions for solving the digital call, call options using RK3-BDF3-BDF4 and CN time-stepping methods. Like before, we use fourth-order FD discretization in space, and no

smoothing modifications are applied to the initial conditions. We choose $h = 0.5$ and $d = \frac{k}{h} = 0.01$ for both examples. The results are plotted in Figure 3. We see that no spurious oscillation occur in the solutions with RK3-BDF3-BDF4 time stepping as expected, due to the high-frequency damping properties of BDF methods.
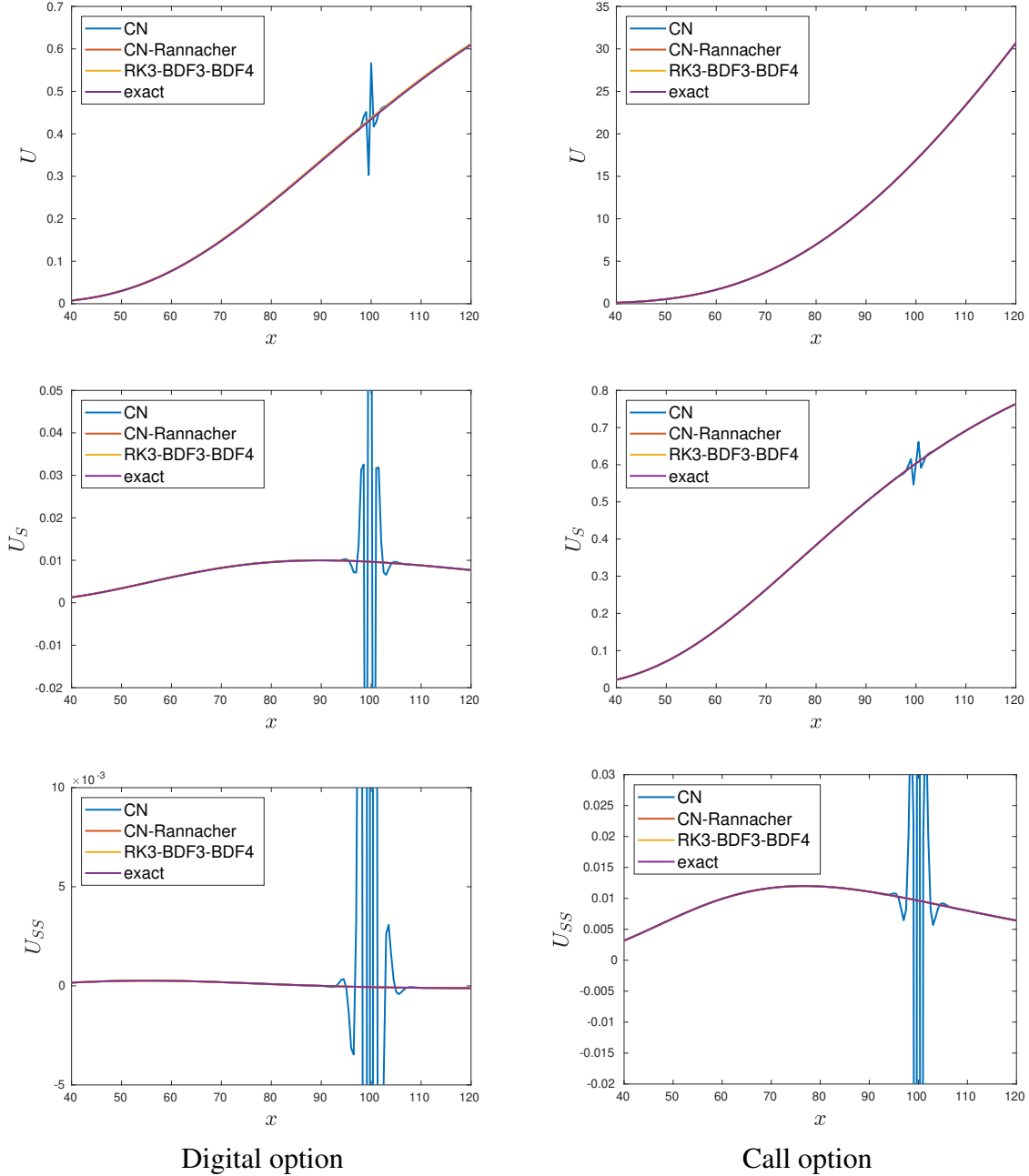

Figure 3: Comparison of numerical solutions and the calculated Δ, Γ of the European digital call and call options, with volatility $\sigma = 0.2$, with CN, CN-Rannacher and RK3-BDF3-BDF4 methods.

(M, N)	α	V			Δ		Γ	
		value	error	conv	error	conv	error	conv
		w/o smoothing						
(40,20)	0.6667	0.568113749	7.43e-02	-	5.35e-04	-	4.21e-04	-
(80,40)	0.3333	0.459075097	3.58e-02	1.05	3.72e-04	0.53	1.91e-04	1.14
(160,80)	0.6667	0.512425925	1.74e-02	1.04	7.59e-05	2.29	8.83e-05	1.11
(320,160)	0.3333	0.486264480	8.76e-03	0.99	1.89e-05	2.01	4.37e-05	1.01
(640,320)	0.6667	0.499382679	4.36e-03	1.01	4.71e-06	2.00	2.18e-05	1.00
		w smoothing						
(40,20)	0.6667	0.500060559	4.55e-03	-	1.23e-03	-	6.22e-05	-
(80,40)	0.3333	0.495628236	6.93e-04	2.71	1.73e-04	2.83	6.17e-06	3.33
(160,80)	0.6667	0.495075147	5.29e-05	3.71	1.08e-05	4.00	6.79e-07	3.18
(320,160)	0.3333	0.495028135	3.46e-06	3.94	6.89e-07	3.98	4.50e-08	3.91
(640,320)	0.6667	0.495025124	2.20e-07	3.98	4.32e-08	4.00	2.90e-09	3.96

Table 6: Convergence results for the price V and its Δ and Γ at the strike $K = 100$, for solving the European digital option, taking $\sigma = 0.2$. The grid alignment value α varies on each grid refinement level as given in the table.

(M, N)	α	V			Δ		Γ	
		value	error	conv	error	conv	error	conv
		w/o smoothing						
(40,20)	0.6667	22.706368799	4.61e-02	-	4.66e-05	-	1.45e-05	-
(80,40)	0.3333	22.670339162	1.00e-02	2.20	5.39e-05	-0.21	3.33e-06	2.12
(160,80)	0.6667	22.663038447	2.70e-03	1.89	1.10e-05	2.29	9.06e-07	1.88
(320,160)	0.3333	22.660991961	6.50e-04	2.05	3.20e-06	1.78	2.19e-07	2.05
(640,320)	0.6667	22.660507365	1.66e-04	1.97	7.54e-07	2.09	5.58e-08	1.97
		w smoothing						
(40,20)	0.6667	22.659843234	5.96e-04	-	4.44e-05	-	1.59e-06	-
(80,40)	0.3333	22.660297803	3.78e-05	3.98	3.00e-06	3.89	3.67e-08	5.44
(160,80)	0.6667	22.660338994	2.61e-06	3.85	2.02e-07	3.90	2.76e-09	3.73
(320,160)	0.3333	22.660341607	1.67e-07	3.97	1.26e-08	4.00	1.86e-10	3.89
(640,320)	0.6667	22.660341776	1.05e-08	3.99	7.87e-10	4.00	1.14e-11	4.02

Table 7: Convergence results for the price V and its Δ and Γ at the strike $K = 100$, for solving the European call option, taking $\sigma = 0.8$. The grid alignment value α varies on each grid refinement level as given in the table.

9   Conclusions

In this paper, we have developed and analyzed a fourth-order method to solve parabolic PDEs with nonsmooth initial conditions. We applied Fourier analysis to a model convection-diffusion PDE and proved that the exponential damping of high-frequency error components using BDF4 makes it a good combination with RK3 as the starting scheme for nonsmooth data, and guarantees fourth-order convergence and stability,

(M, N)	α	V			Δ		Γ	
		value	error	conv	error	conv	error	conv
		$K_1 = 80.25$ (w/o smoothing)						
(40,20)	0.35000	4.108437670	7.78e-02	-	2.81e-02	-	3.21e-03	-
(80,40)	0.70000	4.173066559	5.38e-03	3.85	8.85e-03	1.67	2.44e-04	3.72
(160,80)	0.40000	4.169334971	8.57e-03	-0.67	1.36e-03	2.70	1.76e-04	0.48
(320,160)	0.80000	4.158899648	1.96e-03	2.13	2.70e-04	2.33	1.18e-05	3.89
(640,320)	0.60000	4.161549262	6.98e-04	1.49	5.92e-05	2.19	1.20e-05	-0.02
		$K_1 = 80.25$ (w smoothing)						
(40,20)	0.35000	4.376718594	1.30e-01	-	2.08e-02	-	4.65e-03	-
(80,40)	0.70000	4.176683715	1.22e-02	3.42	4.26e-03	2.29	3.03e-04	3.94
(160,80)	0.40000	4.161766412	7.92e-04	3.94	3.65e-04	3.55	1.79e-05	4.08
(320,160)	0.80000	4.160905971	5.05e-05	3.97	2.25e-05	4.02	1.15e-06	3.96
(640,320)	0.60000	4.160854034	3.18e-06	3.99	1.41e-06	3.99	7.23e-08	3.99
		$K_2 = 100$ (w/o smoothing)						
(40,20)	0.66667	9.096127563	2.38e-01	-	3.50e-02	-	4.30e-04	-
(80,40)	0.33333	9.338618860	9.71e-02	1.29	3.85e-03	3.19	1.65e-04	1.38
(160,80)	0.66667	9.415269963	2.22e-02	2.13	9.68e-04	1.99	1.13e-04	0.54
(320,160)	0.33333	9.431223427	6.43e-03	1.79	7.37e-05	3.72	2.29e-05	2.31
(640,320)	0.66667	9.436768375	8.96e-04	2.84	2.05e-05	1.85	9.74e-06	1.23
		$K_2 = 100$ (w smoothing)						
(40,20)	0.66667	9.174877799	1.71e-01	-	5.18e-02	-	2.02e-03	-
(80,40)	0.33333	9.425482368	8.49e-03	4.33	5.34e-04	6.60	2.71e-04	2.90
(160,80)	0.66667	9.436777317	6.97e-04	3.61	6.86e-05	2.96	1.91e-05	3.83
(320,160)	0.33333	9.437610473	4.71e-05	3.89	4.96e-06	3.79	1.25e-06	3.94
(640,320)	0.66667	9.437661793	2.97e-06	3.99	3.12e-07	3.99	7.89e-08	3.98
		$K_3 = 119.75$ (w/o smoothing)						
(40,20)	0.98333	4.246070790	6.30e-01	-	6.19e-03	-	2.36e-03	-
(80,40)	0.96667	4.725424517	1.49e-01	2.08	3.03e-03	1.03	3.76e-04	2.65
(160,80)	0.93333	4.849020081	2.58e-02	2.53	5.97e-04	2.34	4.26e-05	3.14
(320,160)	0.86667	4.870124235	4.73e-03	2.45	1.82e-04	1.72	1.38e-06	4.95
(640,320)	0.73333	4.874586104	2.70e-04	4.13	4.08e-05	2.16	2.30e-06	-0.74
		$K_3 = 119.75$ (w smoothing)						
(40,20)	0.98333	4.813475069	6.06e-02	-	1.73e-02	-	1.09e-03	-
(80,40)	0.96667	4.868931521	5.80e-03	3.39	1.58e-03	3.46	9.69e-05	3.49
(160,80)	0.93333	4.874470837	3.92e-04	3.89	1.06e-04	3.90	6.82e-06	3.83
(320,160)	0.86667	4.874832706	2.46e-05	3.99	6.73e-06	3.97	4.58e-07	3.90
(640,320)	0.73333	4.874854735	1.53e-06	4.01	4.22e-07	3.99	2.89e-08	3.98

Table 8: Convergence results for the price V and its Δ and Γ at the strikes $K_1 = 80.25$, $K_2 = 100$, $K_3 = 119.75$, for solving the butterfly spread option, taking $\sigma = 0.2$. The grid alignment values α vary for all three singular points on each grid refinement level as given in the table.

assuming the nonsmooth initial conditions are discretized to a high-order. Our analysis can be easily extended to even higher order methods in the BDF family. Moreover, we have provided simple explicit

formulas for the discretization of the Dirac delta, Heaviside and ramp initial conditions as a high-order smoothing mechanism, so that the discrete initial conditions are fourth-order accurate in the frequency domain. The numerical results on convection-diffusion PDEs, and European digital call, call and butterfly options show stable fourth-order convergence, and verify the correctness of our analysis. Furthermore, the calculated solution derivatives exhibit fourth-order accuracy. Though this work is developed with Black-Scholes PDE in mind, we note that the contribution of this paper is not only applicable to option pricing problems, but also to more general parabolic PDEs with nonsmooth initial data.

References

[1] J. H. BRAMBLE AND B. E. HUBBARD, *On a finite difference analogue of an elliptic boundary problem which is neither diagonally dominant nor of non-negative type*, J. Math. and Phys., 43 (1964), pp. 117–132.

[2] C. C. CHRISTARA AND N. CHUN-HO LEUNG, *Analysis of quantization error in financial pricing via finite difference methods*, SIAM J. Numer. Anal., 56 (2018), pp. 1731–1757.

[3] M. J. DILLOO AND D. Y. TANGMAN, *A high-order finite difference method for option valuation*, Comput. Math. Appl., 74 (2017), pp. 652–670.

[4] B. DÜRING AND M. FOURNIÉ, *High-order compact finite difference scheme for option pricing in stochastic volatility models*, J. Comput. Appl. Math., 236 (2012), pp. 4462–4473.

[5] B. DÜRING AND C. HEUER, *High-order compact schemes for parabolic problems with mixed derivatives in multiple space dimensions*, SIAM J. Numer. Anal., 53 (2015), pp. 2113–2134.

[6] B. DÜRING AND A. PITKIN, *High-order compact finite difference scheme for option pricing in stochastic volatility jump models*, J. Comput. Appl. Math., 355 (2019), pp. 201–217.

[7] M. B. GILES AND R. CARTER, *Convergence analysis of Crank-Nicolson and Rannacher time-marching*, J. Comput. Finance, 9 (2006), pp. 89–112.

[8] H.-O. KREISS, V. THOMÉE, AND O. WIDLUND, *Smoothing of initial data and rates of convergence for parabolic difference equations*, Comm. Pure Appl. Math., 23 (1970), pp. 241–259.

[9] M.-N. LE ROUX, *Semi-discretisation en temps pour les equations d'evolution paraboliques lorsque l'operateur depend du temps*, RAIRO. Analyse numérique, 13 (1979), pp. 119–137.

[10] C. W. OOSTERLEE, J. C. FRISCH, AND F. J. GASPAR, *TVD, WENO and blended BDF discretizations for Asian options*, Comput. Vis. Sci., 6 (2004), pp. 131–138.

[11] C. W. OOSTERLEE, C. C. LEENTVAAR, AND X. HUANG, *Accurate American option pricing by grid stretching and high order finite differences*, Delft University of Technology, The Netherlands, Technical Report, (2005).

[12] D. M. POOLEY, K. R. VETZAL, AND P. A. FORSYTH, *Convergence remedies for non-smooth payoffs in option pricing*, J. Comput. Finance, 6 (2003), pp. 25–40.

[13] R. RANNACHER, *Finite element solution of diffusion problems with irregular data*, Numerische Mathematik, 43 (1984), pp. 309–327.

[14] C.-W. SHU, *Essentially non-oscillatory and weighted essentially non-oscillatory schemes for hyperbolic conservation laws*, in Advanced numerical approximation of nonlinear hyperbolic equations (Cetraro, 1997), vol. 1697 of Lecture Notes in Math., Springer, Berlin, 1998, pp. 325–432.

[15] D. Y. TANGMAN, A. GOPAUL, AND M. BHURUTH, *Numerical pricing of options using high-order compact finite difference schemes*, J. Comput. Appl. Math., 218 (2008), pp. 270–280.

[16] D. TAVELLA AND C. RANDALL, *Pricing financial instruments: The finite difference method*, vol. 13, John Wiley & Sons, 2000.

[17] L. N. TREFETHEN, *Spectral methods in MATLAB*, vol. 10 of Software, Environments, and Tools, Society for Industrial and Applied Mathematics (SIAM), Philadelphia, PA, 2000.